

An Ultraviolet Investigation of Activity on Exoplanet Host Stars ¹

Evgenya L. Shkolnik

Lowell Observatory, 1400 West Mars Hill Road, Flagstaff, AZ, 86001, USA

shkolnik@lowell.edu

ABSTRACT

Using the far-UV (FUV) and near-UV (NUV) photometry from the NASA Galaxy Evolution Explorer (*GALEX*), we searched for evidence of increased stellar activity due to tidal and/or magnetic star-planet interactions (SPI) in the 272 of known FGK planetary hosts observed by *GALEX*. With the increased sensitivity of *GALEX*, we are able to probe systems with lower activity levels and at larger distances than what has been done to date with X-ray satellites. We compared samples of stars with close-in planets ($a < 0.1$ AU) to those with far-out planets ($a > 0.5$ AU) and looked for correlations of excess activity with other system parameters. This statistical investigation found no clear correlations with a , M_p , nor M_p/a , in contrast to some X-ray and Ca II studies. However, there is tentative evidence (at a level of $1.8\text{-}\sigma$) that stars with RV-detected close-in planets are more FUV-active than stars with far-out planets, in agreement with several published X-ray and Ca II results. The case is strengthened to a level of significance of $2.3\text{-}\sigma$ when transit-detected close-in planets are included. This is most likely because the RV-selected sample of stars is significantly less active than the field population of comparable stars, while the transit-selected sample is similarly active. Given the factor of 2–3 scatter in fractional FUV luminosity for a given stellar effective temperature, it is necessary to conduct a time-resolved study of the planet hosts in order to better characterize their UV variability and generate a firmer statistical result.

Subject headings: stars: exoplanet hosts, stars: late-type, activity

¹Based on observations made with the NASA Galaxy Evolution Explorer. *GALEX* is operated for NASA by the California Institute of Technology under NASA contract NAS5-98034.

1. Introduction

1.1. Magnetic Star-Planet Interactions

Planetary systems characterized by giant planets located a few stellar radii from their parent stars (“hot Jupiters”) make up 20% of all known exoplanetary systems. For these mature hot Jupiter systems several studies (e.g. Shkolnik et al. 2003, 2005, 2008; Saar et al. 2008; Walker et al. 2008; Pagano et al. 2009; Lanza 2009, 2010; Pillitteri et al. 2010) have independently converged on the same scenario: a short-period planet can induce activity on the photosphere and upper atmosphere of its host star, making the star itself a probe of its planet.

The first such monitoring campaign of chromospheric emission from hot Jupiter host stars revealed that stellar activity tracers vary with the planet’s orbital period rather than the star’s rotation for several systems (Shkolnik et al. 2003, 2005; Gurdemir et al. 2012). Pillitteri et al. (2011) reported repeated coronal X-ray flares from HD 189733 at the same orbital phase. These planet-phased phenomena are interpreted as evidence for magnetic star-planet interactions (SPI) induced by the *magnetized* planet (Lanza 2008, 2009; Cohen et al. 2009). The roles of magnetic fields (both stellar and planetary) in the formation and migration of giant planets are currently rarely evoked and never precisely described because of a lack of data and the complexity of the processes involved. In fact, the strength of any exoplanetary fields is completely unknown and only inferred by making comparisons with Jupiter, while direct measurements using radio emission have not yet succeeded (e.g. Lecavelier Des Etangs et al. 2011).

Magnetic SPI in hot Jupiter systems is detectable because the planets in general lie within the Alfvén radius of their parent stars ($\lesssim 10 R_*$). Within this distance, the Alfvén speed is higher than the stellar wind speed, thereby allowing direct magnetic interaction with the stellar surface. If a hot Jupiter is magnetized, its magnetosphere interacts with the open coronal fields of its star throughout its orbital motion, potentially through magnetic reconnection (Lanza 2008, 2009; Cohen et al. 2009), propagation of Alfvén waves within the stellar wind (Preusse et al. 2006; Kopp et al. 2011), and/or the generation of an electron beam which strikes the base of a stellar corona (Gu & Suzuki 2009). Lanza (2011) considers also a planetary magnetic field with more realistic, non-uniform stellar magnetic field configurations in order to explain possible evidence for SPI as revealed by the photospheric magnetic activity in some of the CoRoT planet hosts.

These studies demonstrate the need to understand the host star’s magnetic field and activity. The existing models of magnetic SPI generally give a dissipated power P_d depending on the coronal field strength B_* , the strength of the planetary field B_p , and the relative

velocity of the planet with respect to the coronal field lines v . Considering the treatment of Lanza (2009), this gives a dissipated power of

$$P_d \propto B_*^{4/3} B_p^{2/3} v \quad (1)$$

Since the strength of the stellar field can be derived from spectropolarimetric measurements or estimated from spectroscopic activity/rotation diagnostics (e.g. Collier Cameron & Jianke 1994; Fares et al. 2012), and the orbital parameters of the systems are known, we can derive relative values of the planetary field strength from observations of the excess power radiated by a chromospheric/coronal hot spot (E. Shkolnik, in preparation).

Both the star’s and the planet’s magnetic field need to be of some minimum strength in order for the SPI phenomenon to be observed. This explains the null detection of planet-phased stellar activity on WASP-18 by Miller et al. (2012), since the star has an extremely weak field based on the fact that it is the least active, i.e. has the lowest $\log(R'_{HK})$,¹ of all known planets hosts. Conversely, the HD 189733 system has the strongest detected SPI emission to date (Shkolnik et al. 2008) as well as the strongest stellar magnetic field measurement of 40 G. (Fares et al. 2010).

1.2. Planetary Effects on Stellar Angular Momentum Evolution

It is well-known that main-sequence FGK stars have magnetized stellar winds, which act as brakes to the stellar rotation, and thus decrease the global stellar activity. This produces the useful age-rotation-activity relationships (e.g. Barnes 2007; Mamajek & Hillenbrand 2008). However, in addition to magnetic SPI, tidal interactions in hot Jupiter systems may also increase the star’s activity levels by tidally spinning up the star until the two bodies are tidal locked, e.g. τ Boo, CoRoT-4 (Catala et al. 2007; Aigrain et al. 2008). If a hot Jupiter is affecting the star’s angular momentum, then the age-activity relation of these systems will systematically underestimate the star’s age, rendering “gyrochronology” inapplicable to such systems.

Pont (2009) and Brown et al. (2011) presented empirical evidence for excess rotation of the host stars compared to evolutionary models in several transiting systems presumed to be due to tidal spin-up of the star caused by its planet. Additional evidence of this using two hot Jupiter systems has been reported by Schröter et al. (2011) and Pillitteri et al. (2010,

¹The $\log(R'_{HK})$ index is the ratio of the chromospheric emission of the Ca II H & K lines to the bolometric flux of the star (Noyes et al. 1984).

2011). Both of these studies did not detect X-ray emission from known M dwarf companions to their relatively active planet hosts (CoRoT-2 and HD 189733, respectively). This lack of X-ray emission indicates that the systems are >2 Gyr old (West et al. 2008), but the activity-rotation age of the planet hosts are 100–300 Myr for CoRoT-2 and 600 Myr for HD 189733. These discrepancies would be resolved if the excess rotation and activity on the primaries were due to interactions with the close-in giant planets, and not their proposed youth.

Lanza (2010) showed that tides in these systems may be too weak to spin-up the star, and provided an alternative explanation for the excess stellar rotation. He proposed that interactions between the planetary field and stellar coronal field lead to a stellar magnetic field topology with predominantly closed field lines, thereby limiting the stellar wind flow and consequent angular momentum loss. Lanza adopted an analytic linear force-free model to compute the radial extent of the corona and its angular momentum loss rate. He found that stars with magnetized hot Jupiters experience angular momentum loss at a significantly slower pace than similar stars without such massive planets. This reduction in angular momentum loss due to the interaction between the stellar and planetary magnetic fields is confirmed by the MHD calculations of Cohen et al. (2009, 2010) and Vidotto et al. (2011).

1.3. Are stars with hot Jupiters more active than stars with cold Jupiters?

As the number of known exoplanets with published orbital parameters begins to climb, statistical studies of the ensemble become an effective and efficient way to study exoplanetary systems. Correlations between stellar activity and planet properties were first shown for a sample of only 13 stars in Shkolnik et al. (2005) and Shkolnik et al. (2008) who showed that short-term variability observed in the chromospheric Ca II H & K emission correlated with the ratio of the minimum planetary mass to the rotational orbital period, a value proportional to the planet’s magnetic field strength (Tholen et al. 2000; Kivelson et al. 2002). More recently Hartman (2010) showed that the Ca II emission, as measured by $\log(R'_{HK})$, of a sample of transiting systems correlates with the planet’s surface gravity, although an explanation is not provided. Knutson et al. (2010) found a correlation between the $\log(R'_{HK})$ of the star and presence of the stratosphere on the planet, likely due to the increased UV flux received by planets orbiting more active stars, which destroys the compounds responsible for the formation of the observed temperature inversions. And most recently, Krejčová & Budaj (2012) presented evidence of larger $\log(R'_{HK})$ for stars with close-in planets compared to stars with far-out planets. This is in agreement with Gonzalez (2011) and yet contrary to Canto Martins et al. (2011).

Over the past few years, a parallel debate in the literature has arisen about correlations between stellar X-ray emission and planet properties. Kashyap et al. (2008) studied the X-ray properties of 46 main-sequence stars with exoplanets. They showed that in a volume-limited sample, those stars with massive planets within 0.15 AU have ≈ 4 times the X-ray emission of those stars with Jupiter-mass planets orbiting with $a > 1.5$ AU. After correction for what they attributed to selection effects, the enhancement was still a factor of two. They speculated that this enhanced activity on the parent star may be induced by magnetic interactions with the close-in giant planet.

Poppenhaeger et al. (2010) repeated a similar X-ray analysis with 72 planet hosts ranging from F to M stars (including main-sequence and giant stars), but did not see the same effect in two samples: $a < 0.2$ AU and $a \geq 0.5$ AU. However, a significant correlation did appear between X-ray luminosity and the ratio between the planet mass and semi-major axis ($M_p \sin i / a$), i.e. massive, close-in planets do tend to orbit more X-ray luminous stars. They assume this correlation is due to the selection bias of the radial velocity (RV) planet search method. Scharf (2010) studied a sample of 29 exoplanet hosts detected by *ROSAT*, and although he saw no significant difference in L_X between two samples, $a < 0.15$ AU and $a > 1.5$ AU, he did report a striking correlation between L_X and $M_p \sin i$ in the first sample. Poppenhaeger & Schmitt (2011) showed that this result is likely due to the selection effects of the flux limit of the X-ray data used and possibly the intrinsic planet detectability of the RV method. Indeed it is easier to find smaller and more distant planets around less active stars, however, both Scharf (2010) and Hartman (2010) demonstrate that for at least stars with planets greater than $0.1 M_J$ orbiting within 2 AU, no significant detection bias of the RV method exists.

In this paper we approach the question of whether or not stars with close-in planets statistically have higher-than-expected stellar activity using a different activity diagnostic, FUV and NUV photometry from NASA’s Galaxy Evolution Explorer (*GALEX*; Martin et al. 2005), providing a new resource that enables a major expansion of the study of stellar activity on exoplanets hosts.

2. *GALEX* Observations of Exoplanet Host Stars

The *GALEX* satellite was launched on April 28, 2003 and has imaged approximately 3/4 of the sky simultaneously in two UV bands: near-UV (NUV) 1750–2750 Å and far-UV (FUV) 1350–1750 Å, with angular resolutions of 5'' and 6.5'', respectively, across a 1.25° field of view. The full description of the instrumental performance is presented by Morrissey et al. (2005). In addition to a medium and a deep imaging survey (MIS, DIS), covering 1000 and

100 square degrees, respectively, the *GALEX* mission has produced an All-sky Imaging Survey (AIS) in both UV bands which is archived at the Multi-mission Archive at the Space Telescope Science Institute (MAST).² The NUV and FUV fluxes and magnitudes averaged over the entire exposure are produced by the standard *GALEX* Data Analysis Pipeline (ver. 4.0) operated at the Caltech Science Operations Center (Morrissey et al. 2007). The data presented in this paper made use of the sixth data release (GR6), which includes the three surveys plus publicly available data from Guest Investigator (GII) programs.

For stars hotter than about 5250 K, the flux in the *GALEX* bandpasses is made up predominantly from continuum emission (Smith & Redenbaugh 2010) with additional flux provided by strong emission lines (C IV, C II, Si IV, He II) originating from the corona, transition region and chromosphere. Cooler stars have FUV and NUV fluxes strongly dominated by stellar activity (e.g. Robinson et al. 2005; Welsh et al. 2006; Pagano 2009). This makes *GALEX* an excellent tool with which to study stellar activity, especially since *GALEX* can detect FGK (and early Ms) at great distances than the existing X-ray missions, out to ~ 150 pc for the FUV and between 20 and 500 pc, depending of T_{eff} for the NUV (Findeisen & Hillenbrand 2010; Shkolnik et al. 2011).

2.1. The Sample

As of November 2012, orbital parameters of 641 extrasolar planets orbiting 523 stars were published in the literature, and conveniently compiled in the Exoplanet Data Explorer (<http://www.exoplanets.org>; Wright et al. 2011). We cross-matched this sample of planet hosts against the *GALEX* archive using a $30''$ search radius. We limit our analysis to only F, G, and K stars (T_{eff} between 4500 and 6700 K) that do not have stellar companions within the *GALEX* PSF diameter ($30''$). A histogram of the semi-major axes of the inner-most planets around stars observed by *GALEX* is shown in Figure 1.³ The median positional offset was only $1.9''$, small compared to the reported pointing error of $10''$.

²One can query the *GALEX* archive through either CasJobs (<http://mastweb.stsci.edu/gcasjobs/>) or a web tool called GalexView (<http://galex.stsci.edu/galexview/>).

³The bimodal distribution of the semi-major axis distribution is due to a combination of both astrophysical effects and selection biases. The outer boundary drops off due to the incompleteness of RV surveys. The inner peak around 0.03 AU is likely due to the selection biases of finding lower mass planets closer in to the star and the inherently high frequency of lower-mass planets. And the peak between 1 and 2 AU is explained by Alexander & Pascucci (2012) as being possibly due to the protoplanetary disk clearing by photoevaporation.

Table 1 lists the relevant data for each star observed by *GALEX* as part of the GR6 data release including FUV and NUV fluxes, F_{FUV} and F_{NUV} , and fractional luminosities (L_{FUV}/L_{bol} and L_{NUV}/L_{bol}). The reported fluxes use the *auto* aperture of the *GALEX* pipeline and are deemed reliable as long as they agree to within 20% with the pipeline’s *aper_7* aperture (Morrissey et al. 2007). There are many potential artifacts reported by the *GALEX* archive and one needs to be cautious with edge effects, bright star halos, detector ghosts, hot spots and saturation in order to extract reliable photometry.

Of the 272 FGK stars in the sample observed by *GALEX*, all were detected in the NUV bandpass, yet only 82 of them were not saturated or of good photometric quality. Fifty-two of these were detected by the transit method and 30 were discovered with the RV method. As the transit-detected systems tend to lie further away, fewer of them are saturated. Those detected with the RV method are closer and brighter, and thus the unsaturated NUV detections tend to lie toward the fainter and cooler end of the distribution ($T_{\text{eff}} < 5500$ K). Only 13 stars have both reliable FUV and NUV detections. The FUV observations provide 128 targets with reliable photometry plus 86 upper limits. This sample is 2–4 times larger than the X-ray samples used by Kashyap et al. (2008), Scharf (2010), and Poppenhaeger et al. (2010).

3. Results

In Figures 2 and 3, we plot the fractional FUV and NUV luminosity, $\log(L_{FUV}/L_{bol})$ and $\log(L_{NUV}/L_{bol})$, for the planet hosts as a function of T_{eff} . The dependence of each on T_{eff} is clear due to the large contribution of photospheric flux in these *GALEX* bandpasses. However, at a given T_{eff} , the scatter spans a factor of 2–3 likely due to differences in intrinsic stellar activity, uncertainties in T_{eff} , and metallicity variations between sources. This distribution of FUV and NUV fluxes is also probably affected by the fact that the data consist of a single observation for each star. Yet we know such stars exhibit stellar activity on both short and long-term time scales, e.g. magnetic braking with age, stellar activity cycles, rotational modulation, and perhaps the SPI effects of known and unknown close-in planets described in Section 1.

In order to search for differences in activity levels with semi-major axis a of a system’s inner-most planet, we separated the sample of exoplanet hosts into two bins: $a \leq 0.1$ AU and $0.5 \leq a \leq 2$ AU. We chose $a \leq 0.1$ AU for the “close-in” planetary systems for two reasons:

- 1) A Jupiter-mass planet within 0.1 AU may tidally spin-up the star with a stellar syn-

chronization time scale less than ~ 10 Gyr. Beyond 0.1 AU, the tidal interaction is so weak that no stellar spin-up is expected. Tidal heating of the stellar upper atmosphere is also unexpected beyond this distance (Cuntz et al. 2000).

2) If any SPI is dominated by magnetic SPI, then the Alfvén radius for sun-like stars of ages $\gtrsim 1$ Gyr is also within 0.1 AU (Preusse et al. 2006), and we therefore do not expect any increased stellar activity due to magnetic interactions between the planet and the star to be observable beyond this distance.

The “far-out” sample is limited by 0.5 AU to make sure uncertainties in Alfvén radii are accommodated while the outer limit of 2 AU shields the analysis from potential observing biases. As mentioned above, past studies have shown that within this distance no significant planet-detection biases exist for the RV-discovered planets with minimum planet mass $M_p \sin i > 0.1 M_J$. Transit detections have been strongly biased towards close-in planets leaving us with no confirmed transiting planets with FUV detections in our far-out sample. This will be aided in the future with Kepler observations which will eventually provide confirmed planets in distant orbits⁴ around stars with UV observations. In fact, recent *GALEX* NUV observations have been carried out of the entire Kepler field so we will be able to revisit these questions for transit-detected planets in the very near future (J. Lloyd, personal communication).

3.1. FUV detections

In the FUV bandpass, we are able to make comparisons with the magnitude-complete and kinematically unbiased sample of the nearest F and G (and some K) dwarfs compiled by the Geneva-Copenhagen survey (GCS; Holmberg et al. 2009). To make the fairest comparisons between samples, we removed close binaries and giants, and also limited the metallicity range of the GCS sample to that of the planet hosts: $-0.25 < [\text{Fe}/\text{H}] < 0.6$. Of the remaining stars, 1141 have reliable FUV detections.

Of the known planet hosts, there are 34 stars with reliable FUV detections in the “close-in” sample, of which 18 are detected with the RV method and 16 with the transit method. The “far-out” sample consists of 44 stars all detected with the RV method. Upper limits are also provided for 86 of the transit-detected systems who generally lie further away from the Sun than the brighter, RV-detected systems.

⁴To date, three Kepler planets have been confirmed with $a > 0.5$ AU, one of which has been observed with *GALEX*, but only an upper limit is provided in the FUV.

We searched for activity differences between the close-in and far-out samples, as well as for correlations in the excess FUV emission with planetary system properties to compare with those previously published in the literature using X-ray detections. In order to do this, we removed the FUV temperature dependence by fitting the following second-order polynomial the GCS sample:

$$\log(L_{FUV}/L_{bol}) = 12.584 - 0.0076604T_{\text{eff}} + 7.6091e^{-7}T_{\text{eff}}^2 \quad (2)$$

We then searched for correlations between the residual FUV luminosities ($\Delta\log(L_{FUV}/L_{bol})$) with planet properties, namely $\log(a)$, M_p , and M_p/a for the close-in planets. We find no clear dependence on any of these (Figures 4 and 5) as has been reported in the past using X-ray luminosities (Kashyap et al. 2008; Poppenhaeager et al. 2010; Scharf 2010). This may be due to the difficulties in accurately subtracting the photospheric contribution of the FUV flux, which is not a problem for X-ray studies. X-ray emission is a direct diagnostic of coronal activity alone, whereas the residual FUV flux is composed of emission lines originating in the star’s corona, transition region and chromosphere. In addition, the scatter of the GCS comparison sample spans a factor of 2–3 implying that there are intrinsic stellar variations which are likely drowning out any statistically detectable SPI effects.

When comparing the close-in and far-out samples, a Kolmogorov-Smirnov (K-S) test reveals evidence that the stars with close-in planets do indeed have higher levels of FUV emission compared to stars with far-out planets ($P = 0.022$, $D = 0.31$, $2.3\text{-}\sigma$). And if the same test is done with only the RV-detected planets, the results weaken to $P = 0.077$ ($1.8\text{-}\sigma$), $D = 0.35$. It is important to note that entire sample of RV-detected planet hosts is significantly less active in the FUV than the field population with $P = 0.00$, $D = 0.45$ pointing to the observational bias towards looking for planets around relatively quiescent and slowly rotating stars compared to the field. On the other hand, the FUV detections of transit-detected systems, all of which host planets within $a = 0.1$ AU, are indistinguishable from the field sample with $P = 0.57$, $D = 0.19$ and are notably more active than the RV-selected sample. This is also apparent in the comparison of the $\log(R'_{\text{HK}})$ values of the RV and transit samples where $P = 0.013$, $D = 0.42$. This points to the relative lack of selection bias toward inactive stars of the transit method compared to RV method. This is expected as only a few RVs are necessary to confirm the transiting planet candidate, nor will the RV signal be attributed to stellar activity when the period and phasing is already determined by the transit. Therefore stars with promising planetary transit signals are followed up by RV observations regardless if they are more active than the typical RV planet search targets and are not subject to same very low-activity criteria.

Even though in general it is easier to find more massive planets around more active stars,

there is a range for which sufficient RV precision is achieved such that the selection effects are minimized (or even non-existent): planets with masses greater than $0.1 M_J$ orbiting within 2 AU (e.g. Hartman 2010; Scharf 2010). Unfortunately, reducing the RV-detected planet sample to these ranges leaves only 9 stars in the close-in sample, making statistical comparison with the FUV detections not very meaningful. However, comparing the published $\log(R'_{HK})$ values of the close-in (22 targets) and far-out samples (81 targets) does not yield a significant difference ($P = 0.242$, $D = 0.24$). This is in agreement with Canto Martins et al. (2011) yet disagrees with Gonzalez (2011).

Although our full data set suggests that stars with closer-in planets are be more active than stars with far-out planets, it remains highly probable that this is due to the selection biases of the planet detection methods. More studies designed specifically to address this question are required. It is necessary to conduct a time-resolved study of the planet hosts discovered by a single method in order to better characterize their UV variability.

3.2. NUV detections

A comparison of the exoplanet hosts with the GCS sample is not possible as nearly all of the stars in the GCS sample are saturated in the NUV. In fact, most of the RV-detected planet hosts are also saturated in the NUV as they are typically brighter than the those stars with planets detected using the transit method. However, there are 63 NUV detections of stars with transit detected planets (Figure 3), all with planets within 0.1 AU. As we showed in Section 3.1, the transit sample is comparable in activity levels to the field using the FUV observations and thus we fitted a polynomial to the NUV detections of the transit sample only to remove the T_{eff} dependence. The function is:

$$\log(L_{NUV}/L_{bol}) = -11.491 + 0.0016817T_{\text{eff}} - 5.4353e^{-8}T_{\text{eff}}^2 \quad (3)$$

We searched the residual NUV flux ($\Delta\log(L_{NUV}/L_{bol})$) of the transit systems for correlations with planet properties $\log(a)$, M_p , and M_p/a . Again, no clear correlations were observed (Figures 6 and 7). Clearer answers may emerge from the forthcoming analyses of the dedicated multi-epoch and deep *GALEX*/NUV observations of the Kepler candidates (J. Lloyd, personal communication) which include a wide range of semi-major axes (Batalha et al. 2012).

4. Summary

Using the FUV and NUV photometry the *GALEX* surveys, we searched for evidence of increased stellar activity due to tidal and/or magnetic SPI in the 272 planetary systems observed by *GALEX*. With the increased sensitivity of *GALEX*, we are able probe systems with lower activity levels and at larger distances than what has been done to date with X-ray satellites.

After correcting for the FUV and NUV dependence on T_{eff} , we compared samples of stars with close-in planets ($a < 0.1$ AU) to those with far-out planets ($0.5 < a < 2$ AU) and looked for correlations of activity with other system parameters, i.e. a , M_p , and M_p/a . This statistical investigation found no clear correlations in either the RV-detected or transit-detected samples. However, there is tentative evidence ($1.8\text{-}\sigma$) that stars with RV-detected close-in planets are more FUV-active than stars with far-out planets, in agreement with several published X-ray and Ca II results. The case is strengthened to $2.3\text{-}\sigma$ when transit-detected close-in planets are included. This is most likely a result of the fact that the RV-selected sample of stars is significantly less active than the field population of comparable stars while the transit-selected sample is similarly active.

Even by limiting samples to a range where selection biases are not significant, the single-visit nature of all-sky UV and X-ray surveys pose a problem to such samples as they record only a snapshot observation per star, and do not account for changes in intrinsic stellar activity levels. With a factor of 2–3 scatter in fractional FUV luminosity for a given T_{eff} , it is necessary to conduct a time-resolved study of the planet hosts in order to better characterize their UV variability and generate a firmer statistical result. With the recent completion of a dedicated *GALEX*-NUV multi-epoch survey of the *Kepler* field, we will be able to re-evaluate these results with a much larger, and less biased, dataset.

E.S thanks stimulating discussion with G. Anglada-Escudé, A. C. Cameron, A.N. Lanza, A. Weinberger, K. R. Covey and T. Barman. Also thanks to the *GALEX*/MAST archive developers for their quick responses to all queries. This material is based upon work supported by the NASA/*GALEX* grant program under Cooperative Agreement No. NNX12AC19G issued through the Office of Space Science. This research has made use of the VizieR catalogue access tool, CDS, Strasbourg, France (Ochsenbein et al. 2000).

REFERENCES

- Aigrain, S., et al. 2008, *A&A*, 488, L43
- Alexander, R. D., & Pascucci, I. 2012, *MNRAS*, 422, L82
- Barnes, S. A. 2007, *ApJ*, 669, 1167
- Batalha, N. M., et al. 2012, *ArXiv e-prints*
- Brown, D. J. A., Collier Cameron, A., Hall, C., Hebb, L., & Smalley, B. 2011, *MNRAS*, 415, 605
- Canto Martins, B. L., Das Chagas, M. L., Alves, S., Leão, I. C., de Souza Neto, L. P., & de Medeiros, J. R. 2011, *A&A*, 530, A73+
- Catala, C., Donati, J.-F., Shkolnik, E., Bohlender, D., & Alecian, E. 2007, *MNRAS*, 374, L42
- Cohen, O., Drake, J. J., Kashyap, V. L., Saar, S. H., Sokolov, I. V., Manchester, W. B., Hansen, K. C., & Gombosi, T. I. 2009, *ApJ*, 704, L85
- Cohen, O., Drake, J. J., Kashyap, V. L., Sokolov, I. V., & Gombosi, T. I. 2010, *ApJ*, 723, L64
- Collier Cameron, A., & Jianke, L. 1994, *MNRAS*, 269, 1099
- Cuntz, M., Saar, S. H., & Musielak, Z. E. 2000, *ApJ*, 533, L151
- Desidera, S., et al. 2011, *A&A*, 533, A90
- Eggleton, P. P., & Tokovinin, A. A. 2008, *MNRAS*, 389, 869
- Fares, R., et al. 2012, *ArXiv e-prints*
- . 2010, *MNRAS*, 406, 409
- Findeisen, K., & Hillenbrand, L. 2010, *AJ*, 139, 1338
- Gonzalez, G. 2011, *MNRAS*, 416, L80
- Gu, P.-G., & Suzuki, T. K. 2009, *ApJ*, 705, 1189
- Gurdemir, L., Redfield, S., & Cuntz, M. 2012, *ArXiv e-prints*
- Hartman, J. D. 2010, *ApJ*, 717, L138

- Holmberg, J., Nordström, B., & Andersen, J. 2009, *A&A*, 501, 941
- Kashyap, V. L., Drake, J. J., & Saar, S. H. 2008, *ApJ*, 687, 1339
- Kivelson, M. G., Khurana, K. K., & Volwerk, M. 2002, *Icarus*, 157, 507
- Knutson, H. A., Howard, A. W., & Isaacson, H. 2010, *ApJ*, 720, 1569
- Kopp, A., Schilp, S., & Preusse, S. 2011, *ApJ*, 729, 116
- Krejčová, T., & Budaj, J. 2012, *A&A*, 540, A82
- Lanza, A. F. 2008, *A&A*, 487, 1163
- . 2009, *A&A*, 505, 339
- . 2010, *A&A*, 512, A77+
- . 2011, *Ap&SS*, 658
- Lecavelier Des Etangs, A., Sirothia, S. K., Gopal-Krishna, & Zarka, P. 2011, *A&A*, 533, A50
- Mamajek, E. E., & Hillenbrand, L. A. 2008, *ApJ*, 687, 1264
- Martin, D. C., et al. 2005, *ApJ*, 619, L1
- Masana, E., Jordi, C., & Ribas, I. 2006, *A&A*, 450, 735
- Miller, B. P., Gallo, E., Wright, J. T., & Dupree, A. K. 2012, *ApJ*, 754, 137
- Morrissey, P., et al. 2007, *ApJS*, 173, 682
- . 2005, *ApJ*, 619, L7
- Mugrauer, M., & Neuhäuser, R. 2009, *A&A*, 494, 373
- Noyes, R. W., Hartmann, L. W., Baliunas, S. L., Duncan, D. K., & Vaughan, A. H. 1984, *ApJ*, 279, 763
- Ochsenbein, F., Bauer, P., & Marcout, J. 2000, *A&AS*, 143, 23
- Pagano, I. 2009, *Ap&SS*, 320, 115
- Pagano, I., Lanza, A. F., Leto, G., Messina, S., Barge, P., & Baglin, A. 2009, *Earth Moon and Planets*, 105, 373
- Patience, J., et al. 2002, *ApJ*, 581, 654

- Pillitteri, I., Günther, H. M., Wolk, S. J., Kashyap, V. L., & Cohen, O. 2011, *ApJ*, 741, L18+
- Pillitteri, I., Wolk, S. J., Cohen, O., Kashyap, V., Knutson, H., Lisse, C. M., & Henry, G. W. 2010, *ApJ*, 722, 1216
- Pont, F. 2009, *MNRAS*, 396, 1789
- Poppenhaeger, K., Robrade, J., & Schmitt, J. H. M. M. 2010, *A&A*, 515, A98+
- Poppenhaeger, K., & Schmitt, J. H. M. M. 2011, *ApJ*, 735, 59
- Preusse, S., Kopp, A., Büchner, J., & Motschmann, U. 2006, *A&A*, 460, 317
- Queloz, D., et al. 2010, *A&A*, 517, L1
- Raghavan, D., Henry, T. J., Mason, B. D., Subasavage, J. P., Jao, W.-C., Beaulieu, T. D., & Hambly, N. C. 2006, *ApJ*, 646, 523
- Robinson, R. D., et al. 2005, *ApJ*, 633, 447
- Saar, S. H., Cuntz, M., Kashyap, V. L., & Hall, J. C. 2008, in *IAU Symposium*, Vol. 249, *IAU Symposium*, ed. Y.-S. Sun, S. Ferraz-Mello, & J.-L. Zhou, 79–81
- Scharf, C. A. 2010, *ApJ*, 722, 1547
- Schröter, S., Czesla, S., Wolter, U., Müller, H. M., Huber, K. F., & Schmitt, J. H. M. M. 2011, *A&A*, 532, A3+
- Shkolnik, E., Bohlender, D. A., Walker, G. A. H., & Collier Cameron, A. 2008, *ApJ*, 676, 628
- Shkolnik, E., Walker, G. A. H., & Bohlender, D. A. 2003, *ApJ*, 597, 1092
- Shkolnik, E., Walker, G. A. H., Bohlender, D. A., Gu, P.-G., & Kürster, M. 2005, *ApJ*, 622, 1075
- Shkolnik, E. L., Liu, M. C., Reid, I. N., Dupuy, T., & Weinberger, A. J. 2011, *ApJ*, 727, 6, 12 pp
- Smith, G. H., & Redenbaugh, A. K. 2010, *PASP*, 122, 1303
- Tamuz, O., et al. 2008, *A&A*, 480, L33
- Tholen, D. J., Tejfel, V. G., & Cox, A. N. 2000, *Planets and Satellites*, ed. Cox, A. N., 293

Vidotto, A. A., Jardine, M., Opher, M., Donati, J. F., & Gombosi, T. I. 2011, MNRAS, 412, 351

Walker, G. A. H., et al. 2008, A&A, 482, 691

Welsh, B. Y., et al. 2006, A&A, 458, 921

West, A. A., Hawley, S. L., Bochanski, J. J., Covey, K. R., Reid, I. N., Dhital, S., Hilton, E. J., & Masuda, M. 2008, AJ, 135, 785

Wright, J. T., et al. 2011, PASP, 123, 412

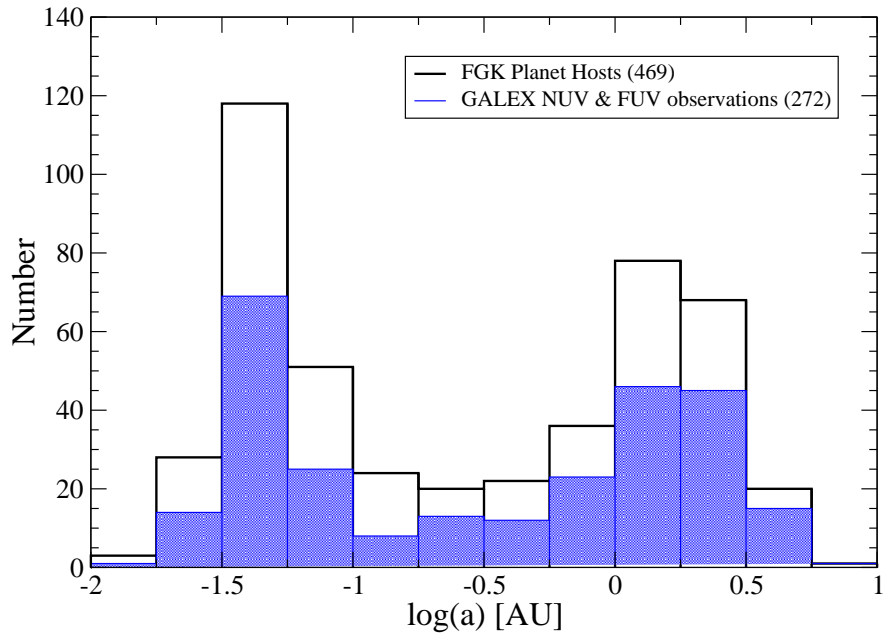


Fig. 1.— A histogram of semi-major axes of the inner-most planet for all confirmed exoplanetary systems ($4500 < T_{\text{eff}} < 6700$ K) to date (black empty bars). Those observed by *GALEX* are shown in blue.

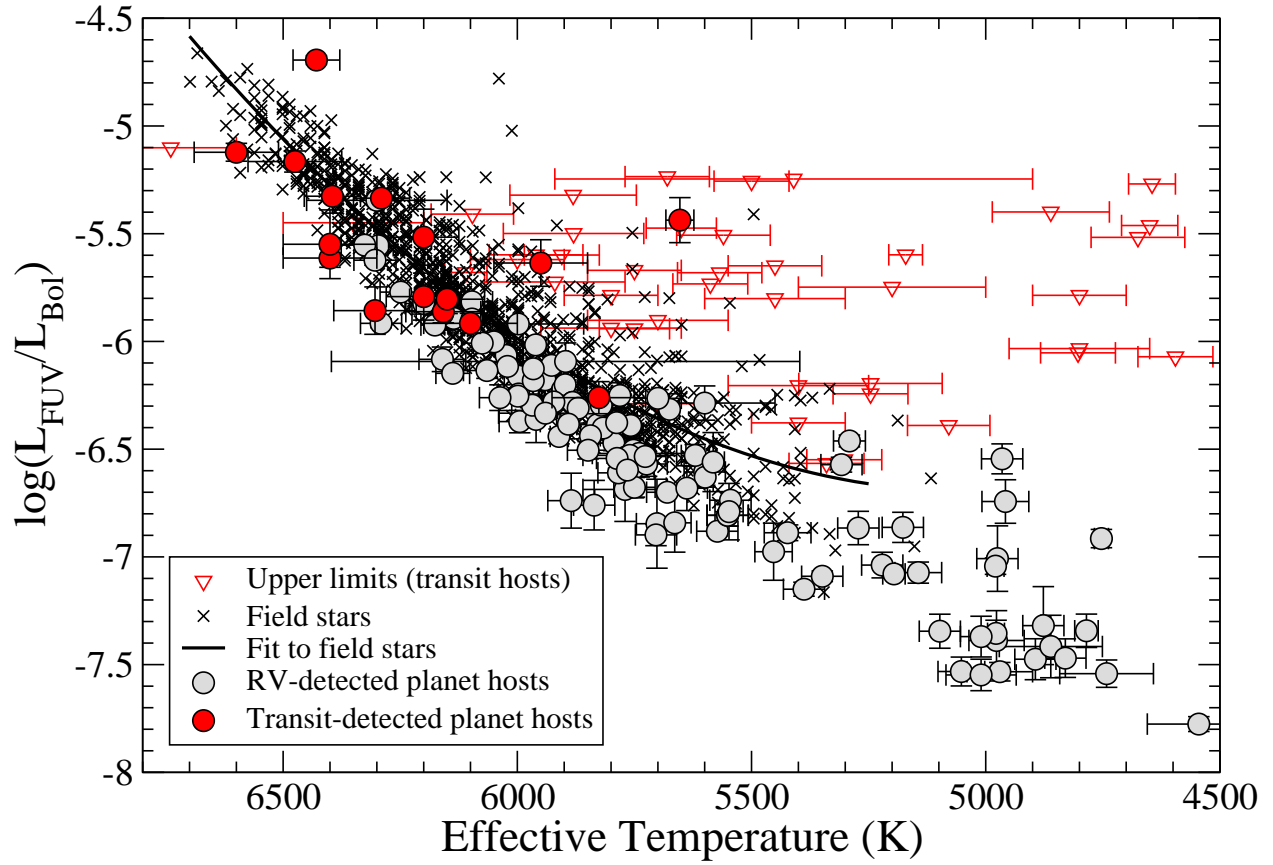


Fig. 2.— The fraction FUV luminosities as a function of effective temperature for RV- (grey) and transit-detected (red) exoplanetary systems. The GCS sample of field stars is shown in black with its the polynomial fit. See text for details.

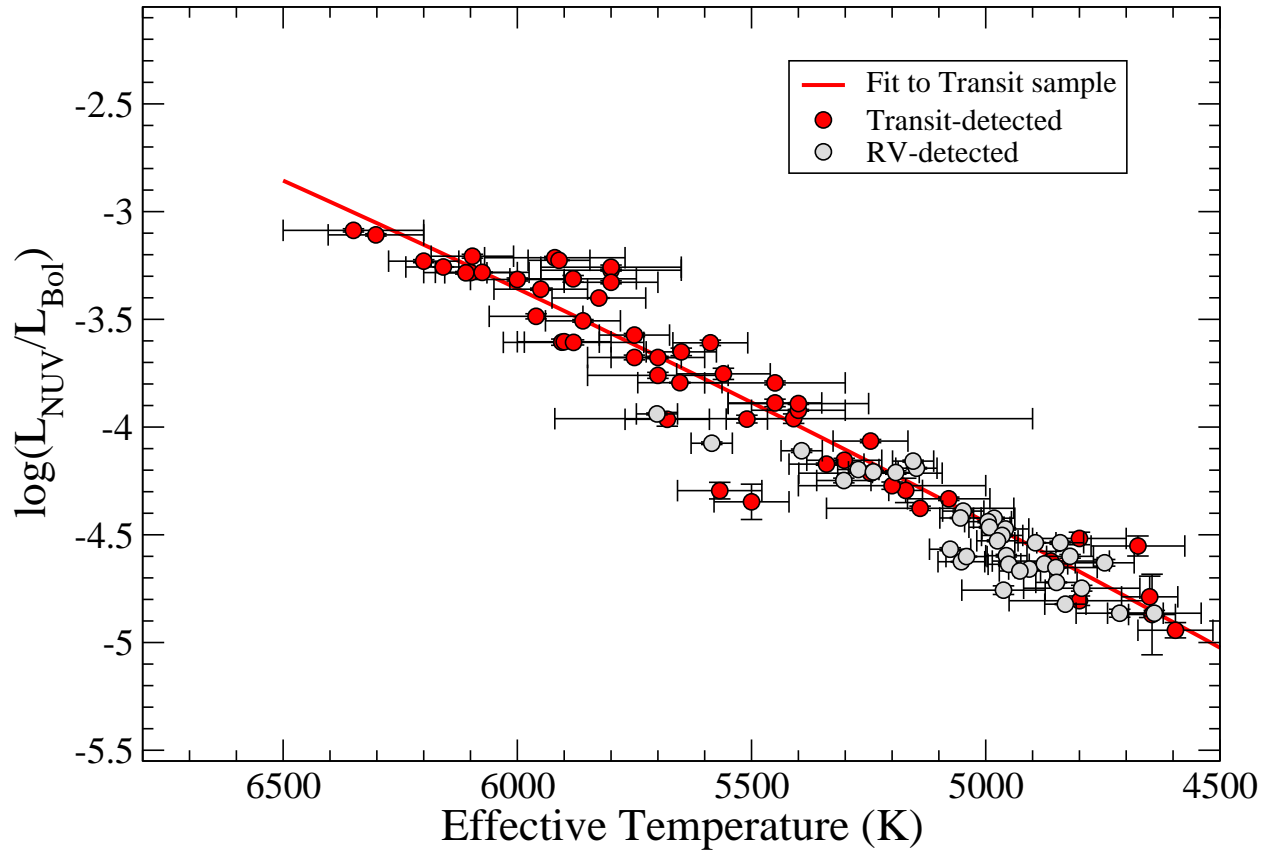


Fig. 3.— The fractional NUV luminosities as a function of effective temperature for exoplanet hosts detected by *GALEX* with good photometry. Most of the RV-detected planet hosts, as well as the GCS field stars, are saturated in the NUV bandpass.

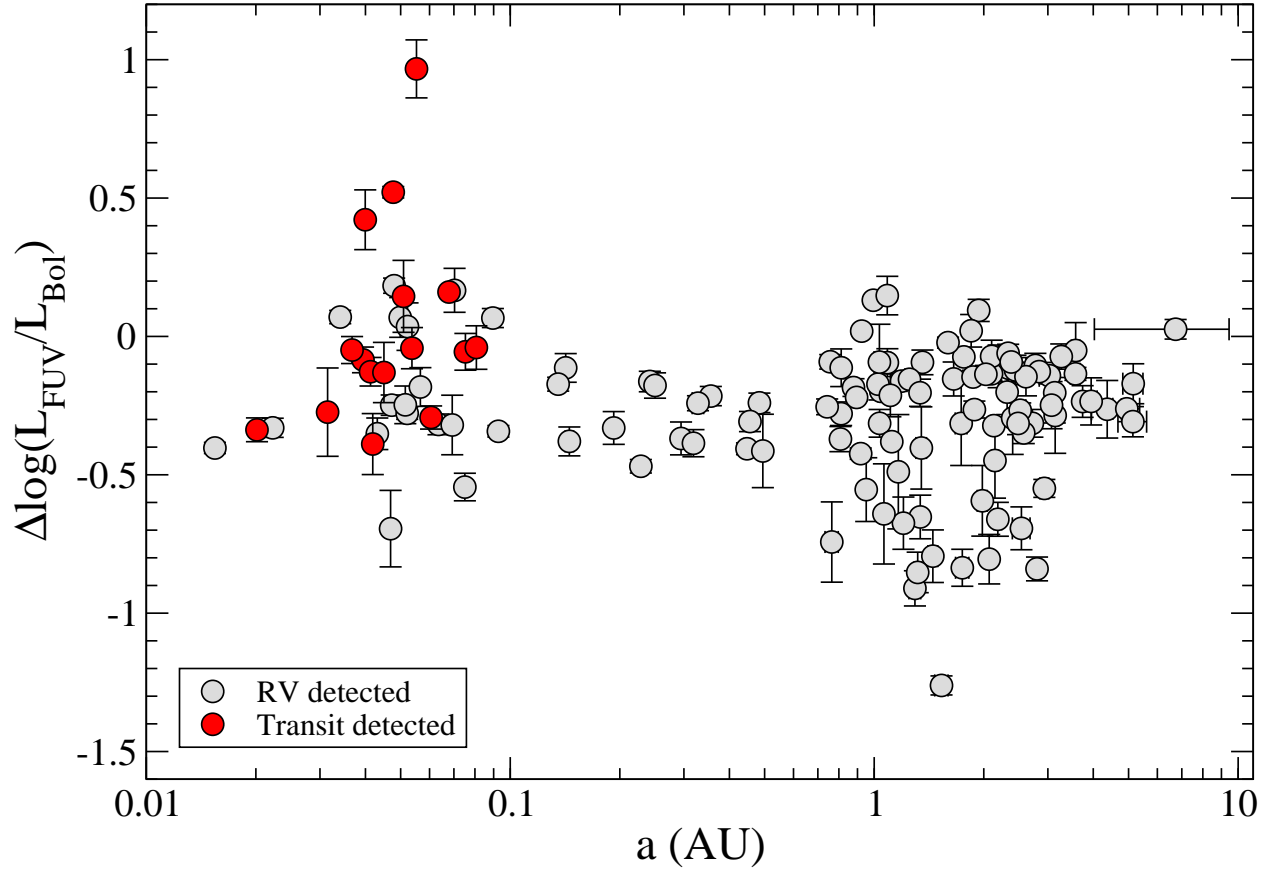


Fig. 4.— Residual FUV luminosities as a function of the semi-major axis of the inner planet mass.

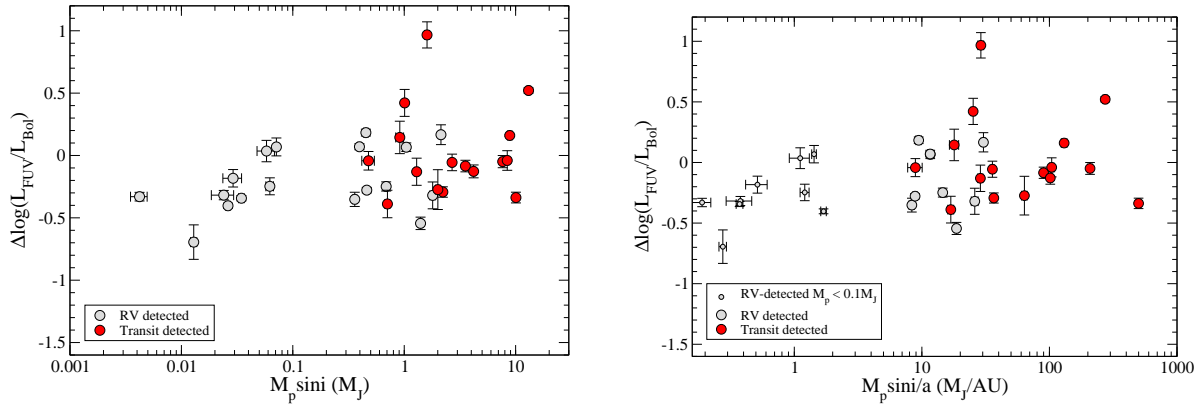


Fig. 5.— The residual fractional FUV luminosity as a function of the mass of the inner most planet for the close-in sample ($a < 0.1$ AU; left) and the ratio of the mass to semi-major axis (right).

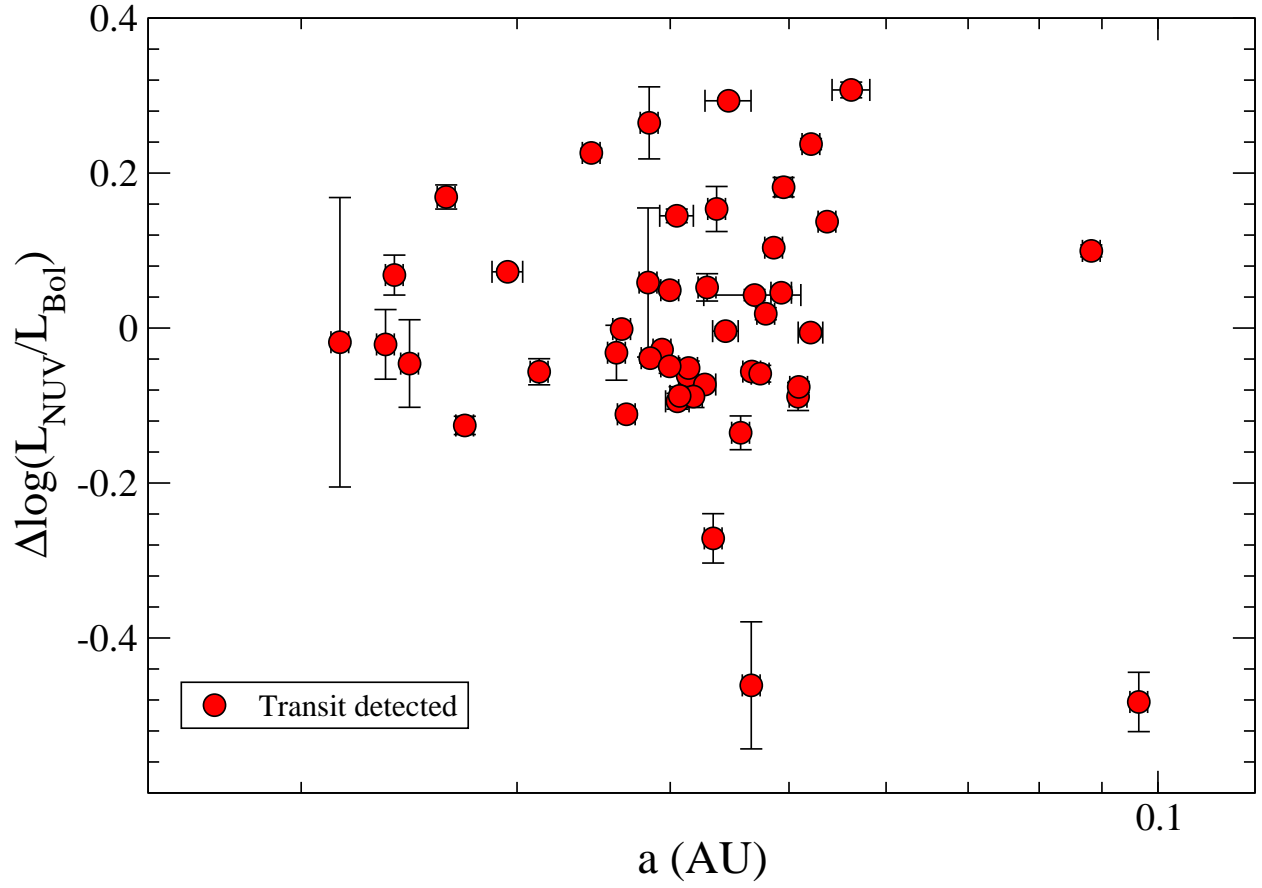


Fig. 6.— Residual NUV luminosities as a function of semi-major axis of inner most planet. Note all transit-detected planets detected by *GALEX* have $a < 0.1$ AU.

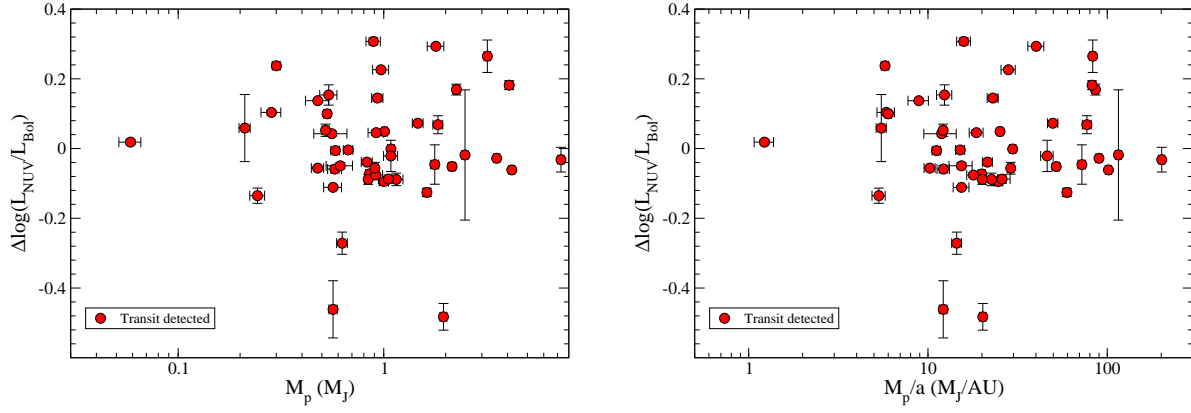


Fig. 7.— The residual fractional NUV luminosity as a function of M_p of the inner most planet (left) and the ratio of the inner planet mass to the semi-major axis (right) for the transit-detected systems. Note all transit-detected planets detected by *GALEX* have $a < 0.1\text{AU}$.

Table 1. Planet and stellar data for *GALEX* detected stars^a

Star/Planet ^a ID	Disc. Method	a^b AU	M_p^b M_J	T_{eff}^b K	<i>GALEX</i> Survey	F_{FUV}^c μJy	F_{NUV}^c μJy	$\log(L_{FUV}/L_{bol})^d$	$\log(L_{NUV}/L_{bol})^d$	NOTE ^e
HD 142 b	RV	1.043	1.31	6249	AIS	855.08 ± 21.77	sat.	-5.771 ± 0.011	–	5.4'' K5 comp. [1]
WASP-44 b	Tran.	0.035	0.89	5410	AIS	< 4	63.06 ± 3.17	< -5.246	-3.961 ± 0.022	NUV artifact
WASP-32 b	Tran.	0.039	3.54	6100	GII	3.54 ± 0.38	1245.32 ± 3.94	-5.916 ± 0.047	-3.283 ± 0.001	
WASP-26 b	Tran.	0.04	1.01	5950	AIS	7.2 ± 1.79	1112.56 ± 12.56	-5.636 ± 0.108	-3.36 ± 0.005	
HD 1461 b	RV	0.064	0.02	5765	AIS	59.18 ± 5.11	sat.	-6.607 ± 0.037	–	
WASP-1 b	Tran.	0.039	0.83	6110	AIS	< 4	816.44 ± 11.7	< -5.68	-3.284 ± 0.006	
WASP-45 b	Tran.	0.041	1	5140	MIS	< 1	57.42 ± 1.35	< -6.223	-4.377 ± 0.01	
HD 2039 b	RV	2.198	5.92	5941	AIS	16.37 ± 2.91	sat.	-6.178 ± 0.077	–	
HIP 2247 b	RV	1.339	5.12	4714	AIS	< 4	249.61 ± 10.67	< -6.746	-4.864 ± 0.019	
HD 2638 b	RV	0.044	0.48	5192	AIS	< 4	1014.9 ± 18.96	< -6.703	-4.211 ± 0.008	
HAT-P-16 b	Tran.	0.041	4.2	6158	NGS	6.21 ± 0.74	2043.47 ± 5.81	-5.862 ± 0.052	-3.257 ± 0.001	
HD 3651 b	RV	0.295	0.23	5221	AIS	44.94 ± 6.16	sat.	-7.038 ± 0.059	–	
HD 4208 b	RV	1.654	0.81	5600	AIS	20.03 ± 2.84	sat.	-6.606 ± 0.061	–	
HD 4203 b	RV	1.165	2.08	5702	AIS	4.83 ± 2.3	3192.77 ± 33.07	-6.846 ± 0.207	-3.939 ± 0.004	
HD 4313 b	RV	1.178	2.35	4991	AIS	–	–	–	–	edge
HAT-P-28 b	Tran.	0.043	0.63	5680	AIS	< 4	61.17 ± 4.49	< -5.235	-3.964 ± 0.032	
HD 5319 b	RV	1.747	1.94	5052	MIS	2.32 ± 0.36	1536.05 ± 4.59	-7.532 ± 0.067	-4.625 ± 0.001	
HD 5388 b	RV	1.763	1.97	6297	AIS	512.5 ± 15.08	sat.	-5.556 ± 0.013	–	
HD 5891 b	RV	0.724	6.78	4907	AIS	< 4	1340.88 ± 16.75	< -7.272	-4.659 ± 0.005	
HD 6434 b	RV	0.142	0.4	5835	AIS	40.51 ± 4.83	sat.	-6.321 ± 0.052	–	
HIP 5158 b	RV	0.888	1.43	4962	AIS	< 4	174.19 ± 8.02	< -6.483	-4.757 ± 0.02	
HD 6718 b	RV	3.554	1.56	5746	AIS	13.56 ± 3.81	sat.	-6.499 ± 0.122	–	bad phot.
HD 7199 b	RV	1.362	0.3	5386	AIS	9.24 ± 3.29	sat.	-6.845 ± 0.155	–	bad phot.
HD 7449 b	RV	2.34	1.31	6024	AIS	86.06 ± 9.78	sat.	-6.065 ± 0.049	–	
HD 7924 b	RV	0.057	0.03	5177	AIS	21.35 ± 3.44	sat.	-6.863 ± 0.07	–	
HD 8535 b	RV	2.445	0.68	6136	AIS	102.58 ± 12.58	sat.	-5.893 ± 0.053	–	
HD 8574 b	RV	0.757	1.81	6050	AIS	138.17 ± 8.34	sat.	-6.002 ± 0.026	–	
HD 9446 b	RV	0.189	0.7	5793	AIS	15.1 ± 3.73	sat.	-6.434 ± 0.107	–	bad phot.
WASP-18 b	Tran.	0.02	10.06	6400	AIS	41.35 ± 4.11	sat.	-5.613 ± 0.043	–	
HD 10180 b	RV	0.022	0	5911	AIS	42.23 ± 3.38	sat.	-6.441 ± 0.035	–	
HD 10697 b	RV	2.132	6.24	5680	GII	64.11 ± 1.48	sat.	-6.7 ± 0.01	–	
HD 11506 b	RV	2.605	4.73	6058	AIS	–	–	–	–	edge
HD 11964 c	RV	0.228	0.08	5349	MIS	24.79 ± 1.39	sat.	-7.09 ± 0.024	–	29.7'' K7 comp. [1]
HD 12661 b	RV	0.838	2.34	5743	AIS	–	–	–	–	edge

Table 1—Continued

Star/Planet ^a ID	Disc. Method	a^b AU	M_p^b M_J	T_{eff}^b K	GALEX Survey	F_{FUV}^c μJy	F_{NUV}^c μJy	$\log(L_{FUV}/L_{bol})^d$	$\log(L_{NUV}/L_{bol})^d$	NOTE ^e
HD 13931 b	RV	5.149	1.88	5829	AIS	37.17 ± 6.18	sat.	-6.386 ± 0.072	-	
HD 16141 b	RV	0.356	0.25	5794	AIS	63.64 ± 5.1	sat.	-6.472 ± 0.035	-	6.2'' M3 comp. [1]
30 Ari B b	RV	0.995	9.88	6300	AIS	636.76 ± 17.95	sat.	-5.345 ± 0.012	-	
HD 16417 b	RV	0.135	0.07	5817	AIS	195.12 ± 11.28	sat.	-6.402 ± 0.025	-	
81 Cet b	RV	2.539	5.34	4785	AIS	32.95 ± 5.87	sat.	-7.343 ± 0.077	-	
HD 16760 b	RV	1.087	13.29	5620	NGS	9.81 ± 1.14	sat.	-6.529 ± 0.05	-	
iota Hor b	RV	0.924	2.05	6097	AIS	1017.78 ± 22.16	sat.	-5.816 ± 0.009	-	
WASP-50 b	Tran.	0.029	1.46	5400	MIS	< 1	233.84 ± 2.23	< -6.378	-3.922 ± 0.004	
HD 18742 b	RV	1.927	2.72	5048	AIS	< 4	2917.28 ± 32.12	< -7.34	-4.39 ± 0.005	
WASP-11 b	Tran.	0.044	0.54	4800	AIS	< 4	60.8 ± 4.07	< -5.786	-4.517 ± 0.029	
HIP 14810 d	RV	1.886	0.58	5485	AIS	9.52 ± 3.55	sat.	-6.631 ± 0.162	-	bad phot.
HD 19994 b	RV	1.306	1.33	6188	MIS	< 1	sat.	< -8.959	-	2.5'' M comp. [1]
HAT-P-25 b	Tran.	0.047	0.57	5500	AIS	< 4	26.55 ± 5.02	< -5.256	-4.347 ± 0.082	
HD 20782 b	RV	1.357	1.76	5758	AIS	47.07 ± 4.85	sat.	-6.39 ± 0.045	-	
HD 20868 b	RV	0.947	2.01	4795	AIS	< 4	210 ± 6.56	< -6.555	-4.748 ± 0.014	
WASP-22 b	Tran.	0.047	0.56	6000	AIS	< 4	660.85 ± 10.96	< -5.62	-3.315 ± 0.007	
epsilon Eri b	RV	3.376	1.05	5146	AIS	< 4	sat.	< -8.964	-	
HD 23127 b	RV	2.319	1.4	5752	AIS	11.43 ± 2.13	sat.	-6.505 ± 0.081	-	
HD 23079 b	RV	1.595	2.44	5927	GII	109.77 ± 5.01	sat.	-6.111 ± 0.02	-	
HD 23596 b	RV	2.772	7.74	5904	AIS	72.8 ± 7.28	sat.	-6.225 ± 0.043	-	
HD 24040 b	RV	4.565	3.84	5853	AIS	35.16 ± 6.27	sat.	-6.456 ± 0.077	-	bad phot.
HD 25171 b	RV	3.031	0.96	6160	AIS	100.72 ± 6.91	sat.	-5.873 ± 0.03	-	
epsilon Ret b	RV	1.267	1.55	4846	AIS	sat.	sat.	-	-	13.8'' faint comp. [1]
HD 27894 b	RV	0.122	0.62	4875	AIS	< 4	438.44 ± 8.99	< -6.762	-4.635 ± 0.009	
XO-3 b	Tran.	0.048	13.05	6429	AIS	210.55 ± 9.97	sat.	-4.694 ± 0.021	-	
HD 28254 b	RV	2.148	1.16	5664	AIS	12.31 ± 3.86	sat.	-6.842 ± 0.136	-	
HAT-P-15 b	Tran.	0.096	1.95	5568	AIS	< 4	79.61 ± 7.02	< -5.681	-4.295 ± 0.038	
HD 28185 b	RV	1.023	5.8	5656	AIS	19.9 ± 4.69	sat.	-6.591 ± 0.102	-	bad phot.
HD 28678 b	RV	1.251	1.71	5076	AIS	< 4	1367.7 ± 21.53	< -7.188	-4.567 ± 0.007	
HD 30177 b	RV	3.808	9.69	5607	AIS	< 4	sat.	< -7.05	-	
HD 30856 b	RV	2.035	1.86	4982	AIS	< 4	2461.03 ± 24.96	< -7.299	-4.423 ± 0.004	
HD 31253 b	RV	1.261	0.5	5960	AIS	-	-	-	-	edge
HD 33283 b	RV	0.145	0.33	5995	AIS	24.8 ± 2.98	sat.	-6.372 ± 0.052	-	
HD 38283 b	RV	1.024	0.34	5998	NGS	144.54 ± 2.43	sat.	-6.161 ± 0.007	-	

Table 1—Continued

Star/Planet ^a ID	Disc. Method	a^b AU	M_p^b M_J	T_{eff}^b K	GALEX Survey	F_{FUV}^c μJy	F_{NUV}^c μJy	$\log(L_{FUV}/L_{bol})^d$	$\log(L_{NUV}/L_{bol})^d$	NOTE ^e
HD 39091 b	RV	3.347	10.09	5950	AIS	355.48 ± 19.2	sat.	$-6.184 \pm$	—	
HD 40307 b	RV	0.047	0.01	4977	AIS	7.39 ± 2.36	sat.	-7.388 ± 0.138	—	
WASP-49 b	Tran.	0.038	0.38	5600	AIS	—	—	—	—	edge
HD 43691 b	RV	0.242	2.5	6200	AIS	66.11 ± 5.64	sat.	-5.824 ± 0.037	—	
HD 44219 b	RV	1.187	0.59	5752	GII	20.92 ± 1.42	sat.	-6.612 ± 0.029	—	bad phot.
HD 45350 b	RV	1.944	1.84	5616	AIS	10.09 ± 2.62	sat.	-6.854 ± 0.113	—	bad phot.
6 Lyn b	RV	2.186	2.21	4978	AIS	24.22 ± 3.42	sat.	-7.355 ± 0.061	—	
HD 47186 b	RV	0.05	0.07	5675	AIS	44.98 ± 7.44	sat.	-6.315 ± 0.072	—	
HD 49674 b	RV	0.057	0.1	5662	AIS	15.09 ± 2.72	sat.	-6.596 ± 0.078	—	bad phot.
HAT-P-9 b	Tran.	0.053	0.78	6350	AIS	< 4	753.74 ± 12.78	< -5.449	-3.087 ± 0.007	NUV artifact
XO-4 b	Tran.	0.055	1.6	5653	AIS	17.55 ± 4.23	sat.	-5.437 ± 0.105	—	
HAT-P-20 b	Tran.	0.036	7.28	4595	AIS	< 4	43.95 ± 3.59	< -6.071	-4.943 ± 0.035	
HD 63454 b	RV	0.036	0.38	4841	AIS	9.65 ± 3.71	565.2 ± 9.22	-6.392 ± 0.167	-4.537 ± 0.007	bad phot.
XO-5 b	Tran.	0.051	1.15	5510	AIS	4.16 ± 1.71	133.84 ± 5.53	-5.558 ± 0.178	-3.963 ± 0.018	bad phot.
XO-2 b	Tran.	0.037	0.57	5340	MIS	< 1	203.11 ± 2.36	< -6.566	-4.172 ± 0.005	
HD 66428 b	RV	3.143	2.75	5752	AIS	13.09 ± 4.13	sat.	-6.589 ± 0.137	—	
HAT-P-35 b	Tran.	0.05	1.05	6096	AIS	< 4	520.81 ± 10.86	< -5.409	-3.207 ± 0.009	NUV artifact
HAT-P-30 b	Tran.	0.042	0.71	6304	AIS	9.09 ± 2.31	sat.	-5.857 ± 0.11	—	
HD 68988 b	RV	0.069	1.8	5960	AIS	22.4 ± 5.55	sat.	-6.362 ± 0.108	—	
HD 69830 b	RV	0.078	0.03	5360	AIS	61.57 ± 6.33	sat.	$-6.864 \pm$	—	
HD 73534 b	RV	3.068	1.1	5041	MIS	3.97 ± 0.68	1329.28 ± 6.23	-7.213 ± 0.074	-4.601 ± 0.002	bad phot.
HAT-P-13 b	Tran.	0.043	0.85	5653	MIS	1.14 ± 0.27	757.79 ± 3.3	-6.703 ± 0.103	-3.794 ± 0.002	bad phot.
WASP-36 b	Tran.	0.026	2.26	5881	AIS	< 4	334.83 ± 11.99	< -5.321	-3.312 ± 0.016	
55 Cnc e	RV	0.015	0.03	5196	MIS	38.95 ± 1.81	sat.	-7.079 ± 0.02	—	
HD 75898 b	RV	1.189	2.52	6021	GII	37.3 ± 1.92	sat.	-6.116 ± 0.022	—	
HD 79498 b	RV	3.133	1.35	5740	AIS	18.69 ± 4.71	sat.	-6.52 ± 0.109	—	
WASP-13 b	Tran.	0.054	0.48	5826	NGS	3.63 ± 0.62	2150.37 ± 7.5	-6.261 ± 0.074	-3.401 ± 0.002	
HD 80606 b	RV	0.447	3.89	5573	NGS	3.31 ± 0.16	2687.28 ± 1.87	-6.881 ± 0.021	-3.885 ± 0	NUV arti.; 20.6'' G5 comp. [1]
HD 81040 b	RV	1.937	6.88	5700	AIS	45.68 ± 4.2	sat.	-6.264 ± 0.04	—	
HD 81688 b	RV	0.811	2.69	4753	AIS	108.8 ± 10.68	sat.	-6.915 ± 0.043	—	
HD 82943 c	RV	0.743	1.99	5997	AIS	135.46 ± 8.87	sat.	-6.244 ± 0.028	—	
HD 82886 b	RV	1.581	1.31	5112	AIS	4.7 ± 1.76	sat.	-7.329 ± 0.163	—	bad phot.
HD 86081 b	RV	0.035	1.5	6028	AIS	20.28 ± 4.77	sat.	-6.193 ± 0.102	—	bad phot.
HD 86264 b	RV	2.841	6.63	6326	AIS	284.96 ± 11.33	sat.	-5.553 ± 0.017	—	

Table 1—Continued

Star/Planet ^a ID	Disc. Method	a^b AU	M_p^b M_J	T_{eff}^b K	GALEX Survey	F_{FUV}^c μJy	F_{NUV}^c μJy	$\log(L_{FUV}/L_{bol})^d$	$\log(L_{NUV}/L_{bol})^d$	NOTE ^e
BD -08 2823 b	RV	0.056	0.05	4746	AIS	< 4	297.25 ± 10.76	< -6.588	-4.63 ± 0.016	
HD 87883 b	RV	3.576	1.76	4958	AIS	21.52 ± 5	3278.87 ± 36.35	-6.743 ± 0.101	-4.473 ± 0.005	
HD 88133 b	RV	0.047	0.3	5494	AIS	6.57 ± 2.05	sat.	-7.009 ± 0.135	-	bad phot.
HD 89307 b	RV	3.266	1.79	5898	AIS	98.65 ± 10.34	sat.	-6.201 ± 0.045	-	
HD 89744 b	RV	0.918	8.47	6291	AIS	593.17 ± 27.85	sat.	-5.916 ± 0.02	-	
HAT-P-22 b	Tran.	0.041	2.15	5302	AIS	< 4	812.93 ± 16.75	< -6.549	-4.154 ± 0.009	
24 Sex b	RV	1.338	1.65	5098	AIS	13.29 ± 2.41	sat.	-7.345 ± 0.079	-	
HD 90156 b	RV	0.25	0.06	5599	AIS	42.25 ± 4.46	sat.	-6.63 ± 0.046	-	
HD 92788 b	RV	0.951	3.56	5836	AIS	21.01 ± 5.58	sat.	-6.76 ± 0.115	-	
HD 93083 b	RV	0.477	0.37	4995	AIS	< 4	1742.92 ± 19.74	< -7.165	-4.439 ± 0.005	
BD -10 3166 b	RV	0.044	0.43	5393	AIS	< 4	666.49 ± 11.91	< -6.418	-4.11 ± 0.008	
HD 95089 b	RV	1.45	1.24	4894	MIS	2.9 ± 0.64	2061.96 ± 7.98	-7.475 ± 0.095	-4.537 ± 0.002	
47 UMa b	RV	2.101	2.55	5882	AIS	490.96 ± 26.52	sat.	-6.283 ± 0.023	-	
47 UMa c	RV	3.572	0.55	5882	AIS	490.96 ± 26.52	sat.	-6.283 ± 0.023	-	
WASP-34 b	Tran.	0.052	0.58	5700	AIS	< 4	1340.11 ± 17.14	< -6.289	-3.677 ± 0.006	
HD 96063 b	RV	0.999	0.92	5148	AIS	9.24 ± 3.66	3062.56 ± 24.98	-6.799 ± 0.172	-4.191 ± 0.004	bad phot.
HD 96167 b	RV	1.347	0.68	5770	AIS	11.9 ± 4.08	sat.	-6.687 ± 0.149	-	
HD 97658 b	RV	0.081	0.02	5170	AIS	9.62 ± 3.4	sat.	-6.98 ± 0.153	-	bad phot.
WASP-31 b	Tran.	0.047	0.48	6302	AIS	5.03 ± 1.79	1283.18 ± 16.4	-5.601 ± 0.154	-3.108 ± 0.006	bad phot.
HD 98219 b	RV	1.23	1.83	4992	AIS	< 4	1953.11 ± 15.88	< -7.241	-4.465 ± 0.004	
HD 99109 b	RV	1.108	0.5	5272	MIS	3.5 ± 0.63	1335.27 ± 4.79	-6.866 ± 0.078	-4.197 ± 0.002	
HAT-P-21 b	Tran.	0.049	4.07	5588	AIS	< 4	436.07 ± 12.6	< -5.733	-3.609 ± 0.013	
HD 99492 b	RV	0.122	0.11	4955	MIS	7.47 ± 0.41	2668.82 ± 4.84	-7.215 ±	-4.575 ±	28.6'' K0 comp. [1]
HD 99706 b	RV	2.134	1.4	4932	AIS	-	-	-	-	edge
HD 100655 b	RV	0.765	1.67	4861	AIS	12.99 ± 4.34	sat.	-7.416 ± 0.145	-	
HD 100777 b	RV	1.034	1.17	5582	AIS	12.26 ± 3.87	sat.	-6.56 ± 0.137	-	
HIP 57274 b	RV	0.071	0.04	4640	AIS	< 4	452.6 ± 13.56	< -7.005	-4.864 ± 0.013	
HD 102195 b	RV	0.048	0.45	5291	MIS	22.85 ± 1.44	sat.	-6.462 ± 0.027	-	
HD 102329 b	RV	2.07	5.87	4830	MIS	3.11 ± 0.64	1131.68 ± 5.63	-7.47 ± 0.089	-4.822 ± 0.002	
HD 102956 b	RV	0.081	0.95	5054	AIS	4.76 ± 1.38	2524.29 ± 13.98	-7.233 ± 0.125	-4.422 ± 0.002	bad phot.
HD 103197 b	RV	0.249	0.1	5303	AIS	< 4	913.37 ± 23.26	< -6.693	-4.248 ± 0.011	
HD 106252 b	RV	2.611	6.96	5870	AIS	53.66 ± 8.55	sat.	-6.31 ± 0.069	-	
HD 106270 b	RV	4.367	11.03	5638	AIS	18.49 ± 4.43	sat.	-6.681 ± 0.104	-	
HD 107148 b	RV	0.27	0.21	5797	AIS	16.84 ± 4.07	sat.	-6.57 ± 0.105	-	bad phot.

Table 1—Continued

Star/Planet ^a ID	Disc. Method	a^b AU	M_p^b M_J	T_{eff}^b K	GALEX Survey	F_{FUV}^c μJy	F_{NUV}^c μJy	$\log(L_{FUV}/L_{bol})^d$	$\log(L_{NUV}/L_{bol})^d$	NOTE ^e
11 Com b	RV	1.294	19.43	4742	AIS	49.14 ± 7.2	sat.	-7.542 ± 0.064	–	10.4'' faint comp. [2]
HD 108863 b	RV	1.398	2.56	4956	AIS	< 4	2029.9 ± 28.96	< -7.389	-4.597 ± 0.006	
HD 108874 b	RV	1.035	1.29	5551	GII	5.12 ± 0.59	sat.	-6.807 ± 0.05	–	
HD 108874 c	RV	2.72	1.03	5551	GII	5.12 ± 0.59	sat.	-6.807 ± 0.05	–	
HD 109246 b	RV	0.328	0.77	5844	GII	11.6 ± 0.72	sat.	-6.438 ± 0.027	–	
HAT-P-36 b	Tran.	0.024	1.83	5560	AIS	< 4	186.07 ± 11.06	< -5.507	-3.753 ± 0.026	
WASP-41 b	Tran.	0.04	0.93	5450	AIS	< 4	331.88 ± 6.72	< -5.801	-3.795 ± 0.009	
WASP-42 b	Tran.	0.055	0.5	5200	AIS	< 4	46.75 ± 5.81	< -5.529	-4.374 ± 0.054	NUV artifact
WASP-25 b	Tran.	0.047	0.58	5750	AIS	< 4	322.44 ± 7.99	< -5.67	-3.677 ± 0.011	
HD 114762 b	RV	0.363	11.64	5953	GII	–	–	–	–	edge; 3.3'' M6 comp. [3]
HD 114783 b	RV	1.16	1.11	5135	AIS	12.73 ± 2.01	sat.	-6.945 ± 0.068	–	bad phot.
HD 114729 b	RV	2.102	0.94	5821	AIS	111.02 ± 14.92	sat.	-6.296 ± 0.058	–	8.1'' faint comp. [1]
61 Vir b	RV	0.05	0.02	5571	AIS	222.15 ± 13.26	sat.	$-6.755 \pm$	–	
HD 116029 b	RV	1.746	2.14	4951	AIS	< 4	1619.7 ± 26.75	< -7.331	-4.637 ± 0.007	
70 Vir b	RV	0.484	7.46	5545	AIS	199.35 ± 16.1	sat.	-6.737 ± 0.035	–	
HD 117207 b	RV	3.738	1.82	5724	AIS	34.34 ± 4.51	sat.	-6.569 ± 0.057	–	
HD 118203 b	RV	0.07	2.14	5600	AIS	31.23 ± 5.71	sat.	-6.286 ± 0.079	–	
Qatar-2 b	Tran.	0.022	2.48	4645	AIS	< 4	8.2 ± 3.53	< -5.269	-4.87 ± 0.187	
HAT-P-12 b	Tran.	0.038	0.21	4650	AIS	< 4	15.48 ± 3.43	< -5.462	-4.788 ± 0.096	
HAT-P-26 b	Tran.	0.048	0.06	5079	MIS	< 1	93.28 ± 1.67	< -6.39	-4.333 ± 0.008	
WASP-16 b	Tran.	0.042	0.84	5700	AIS	< 4	454.55 ± 14.87	< -5.902	-3.76 ± 0.014	
HD 125612 c	RV	0.052	0.06	5897	AIS	25.27 ± 5	sat.	-6.093 ± 0.086	–	
HD 126614 A b	RV	2.368	0.39	5585	AIS	< 4	2170.99 ± 29.77	< -6.897	-4.075 ± 0.006	
WASP-39 b	Tran.	0.049	0.28	5400	MIS	< 1	168.89 ± 1.65	< -6.205	-3.891 ± 0.004	
WASP-14 b	Tran.	0.037	7.65	6475	AIS	82.18 ± 9.24	sat.	-5.165 ± 0.049	–	
HD 128311 b	RV	1.086	1.46	4965	AIS	38.24 ± 6.13	3450.72 ± 37.67	-6.545 ± 0.07	-4.503 ± 0.005	
HD 130322 b	RV	0.09	1.04	5308	MIS	17.64 ± 1.4	sat.	-6.572 ± 0.035	–	
WASP-37 b	Tran.	0.045	1.79	5800	MIS	< 1	379.52 ± 3.47	< -5.938	-3.272 ± 0.004	
HAT-P-27 b	Tran.	0.04	0.61	5246	MIS	< 1	78.31 ± 1.63	< -6.195	-4.214 ± 0.009	
HD 131496 b	RV	2.112	2.24	4927	GII	< 3	1637.43 ± 8.52	< -7.492	-4.668 ± 0.002	
HD 132406 b	RV	1.982	5.6	5885	AIS	10.62 ± 3.12	sat.	-6.739 ± 0.128	–	
HD 132563 B b	RV	2.624	1.49	5985	AIS	70.88 ± 5.38	sat.	-5.423 ± 0.033	–	1.4'' G2 SB comp. [4]
WASP-24 b	Tran.	0.037	1.08	6075	MIS	2.46 ± 0.48	1231.08 ± 5.06	-6.069 ± 0.084	-3.282 ± 0.002	bad phot.
HD 134987 b	RV	0.808	1.56	5750	AIS	55.07 ± 5.78	sat.	-6.677 ± 0.046	–	

Table 1—Continued

Star/Planet ^a ID	Disc. Method	a^b AU	M_p^b M_J	T_{eff}^b K	GALEX Survey	F_{FUV}^c μJy	F_{NUV}^c μJy	$\log(L_{FUV}/L_{bol})^d$	$\log(L_{NUV}/L_{bol})^d$	NOTE ^e
HD 136118 b	RV	2.333	11.68	6097	AIS	210.43 ± 15.67	sat.	-5.896 ± 0.032	–	
HD 136418 b	RV	1.291	1.99	4972	AIS	7.74 ± 2.65	2754.51 ± 21.65	$-10.044 \pm$	-7.406 ± 0.003	NUV artifact
HAT-P-4 b	Tran.	0.044	0.67	5860	AIS	< 4	829.21 ± 11.48	< -5.91	-3.507 ± 0.006	
iota Dra b	RV	1.531	12.72	4545	AIS	121.54 ± 9.62	sat.	-7.776 ± 0.034	–	
HD 137510 b	RV	1.868	26.36	5966	AIS	200.16 ± 11.22	sat.	-6.182 ± 0.024	–	
HD 137388 b	RV	0.889	0.23	5240	AIS	< 4	1873.11 ± 28.09	< -6.966	-4.208 ± 0.007	
kappa CrB b	RV	2.801	2.01	4970	AIS	47.37 ± 4.68	sat.	-7.533 ± 0.043	–	23.2'' faint comp. [2]
HD 142245 b	RV	2.776	1.89	4878	AIS	–	–	–	–	edge
rho CrB b	RV	0.226	1.06	5823	AIS	< 4	sat.	< -8.252	–	
XO-1 b	Tran.	0.049	0.92	5750	AIS	< 4	764.11 ± 13.01	< -5.941	-3.573 ± 0.007	
HD 145457 b	RV	0.763	2.97	4757	AIS	10.2 ± 3.93	sat.	-7.497 ± 0.167	–	bad phot.
14 Her b	RV	2.934	5.21	5388	MIS	17.7 ± 1.32	sat.	-7.15 ± 0.032	–	
WASP-38 b	Tran.	0.075	2.69	6150	AIS	25.65 ± 3.93	sat.	-5.804 ± 0.066	–	
HAT-P-2 b	Tran.	0.068	8.86	6290	GII	142.43 ± 3.02	sat.	-5.335 ± 0.009	–	
HD 149026 b	RV	0.043	0.36	6160	AIS	43.2 ± 5.68	sat.	-6.083 ± 0.057	–	
HD 150706 b	RV	6.734	2.84	5961	AIS	149.05 ± 12.16	sat.	-6.016 ± 0.035	–	
HD 152581 b	RV	1.489	1.51	5155	AIS	5.66 ± 2.68	2874.63 ± 30.81	$-6.951 \pm$	-4.158 ± 0.005	bad phot.
HD 154345 b	RV	4.214	0.96	5468	AIS	21.94 ± 5.38	sat.	$-6.986 \pm$	–	
HAT-P-18 b	Tran.	0.056	0.2	4803	MIS	< 1	40.31 ± 0.95	< -6.053	-4.361 ± 0.01	NUV artifact
HD 155358 b	RV	0.627	0.82	5760	AIS	152.38 ± 11.03	sat.	-5.919 ± 0.031	–	blend
HD 156279 b	RV	0.495	9.78	5453	AIS	6.71 ± 2.05	sat.	-6.976 ± 0.133	–	
HD 156668 b	RV	0.05	0.01	4850	MIS	< 1	1062.76 ± 5.9	< -7.765	-4.652 ± 0.002	
HAT-P-14 b	Tran.	0.061	2.22	6600	AIS	72.56 ± 6.97	sat.	-5.122 ± 0.042	–	
HD 156846 b	RV	1.118	11.01	6138	GII	173.63 ± 2.83	sat.	-6.148 ± 0.007	–	5.1'' M4 comp. [5]
mu Ara d	RV	0.093	0.03	5784	AIS	215.35 ± 10.35	sat.	-6.61 ± 0.021	–	
TrES-3 b	Tran.	0.023	1.87	5650	AIS	< 4	217.94 ± 8.73	< -5.474	-3.651 ± 0.017	NUV artifact
TrES-4 b	Tran.	0.051	0.91	6200	AIS	6.73 ± 2.01	1066.8 ± 17.25	-5.516 ± 0.13	-3.23 ± 0.007	
HD 163607 b	RV	0.359	0.77	5543	AIS	15.46 ± 4.13	sat.	-6.592 ± 0.116	–	bad phot.
HD 164509 b	RV	0.878	0.48	5922	GII	27.4 ± 2.02	sat.	-6.281 ± 0.032	–	
HD 167042 b	RV	1.317	1.7	5010	AIS	15.67 ± 2.64	sat.	-7.548 ± 0.073	–	
HAT-P-5 b	Tran.	0.041	1.05	5960	AIS	< 4	423.48 ± 11.62	< -5.598	-3.486 ± 0.012	
WASP-58 b	Tran.	0.056	0.89	5800	AIS	< 4	988.12 ± 23.03	< -5.738	-3.258 ± 0.01	
HD 170469 b	RV	2.235	0.67	5810	AIS	12.21 ± 4.41	sat.	-6.677 ± 0.157	–	bad phot.
WASP-3 b	Tran.	0.031	2	6400	AIS	15.28 ± 5.62	sat.	-5.549 ± 0.16	–	

Table 1—Continued

Star/Planet ^a ID	Disc. Method	a^b AU	M_p^b M_J	T_{eff}^b K	GALEX Survey	F_{FUV}^c μJy	F_{NUV}^c μJy	$\log(L_{FUV}/L_{bol})^d$	$\log(L_{NUV}/L_{bol})^d$	NOTE ^e
HD 175167 b	RV	2.401	7.78	5548	AIS	10.67 ± 3.23	sat.	-6.79 ± 0.131	–	
Kepler-30 b	Tran.	0.186	0	5498	AIS	< 4	11.95 ± 3.2	< incomplete	incomplete	
Kepler-38 b	Tran.	0.43		5623	GII	< 3	0.93 ± 0.35	< incomplete	incomplete	bad phot.
Kepler-14 b	Tran.	0.081	8.41	6395	GII	7.01 ± 1.27	1268.88 ± 4.33	-5.326 ± 0.079	-2.981 ± 0.001	NUV artifact
HD 179079 b	RV	0.12	0.08	5724	AIS	20.31 ± 4	sat.	-6.523 ± 0.085	–	bad phot.
Kepler-7 b	Tran.	0.062	0.44	5933	GII	< 3	199.55 ± 1.5	< incomplete	incomplete	
HD 179949 b	RV	0.044	0.9	6168	AIS	–	–	–	–	edge
Kepler-33 b	Tran.	0.068		5904	AIS	< 4	61.59 ± 4.73	< -4.879	-3.605 ± 0.033	NUV artifact
Kepler-22 b	Tran.	0.849	0	5518	AIS	< 4	490.32 ± 11.27	< incomplete	incomplete	
HD 180902 b	RV	1.378	1.56	4975	AIS	< 4	2341.31 ± 22.26	< -7.382	-4.528 ± 0.004	NUV artifact
HD 181342 b	RV	1.734	3	4975	AIS	10.2 ± 3.57	2136.88 ± 24.7	-7.008 ± 0.152	-4.6 ± 0.005	NUV artifact
HD 181720 b	RV	1.847	0.37	5781	AIS	38.95 ± 5.29	sat.	-6.251 ± 0.059	–	
WASP-48 b	Tran.	0.034	0.97	5920	AIS	< 4	1059.54 ± 14.52	< -5.724	-3.214 ± 0.006	
Kepler-36 b	Tran.	0.115		5911	GII	< 3	780.62 ± 3	< -5.728	-3.226 ± 0.002	
Kepler-28 b	Tran.	0.058	0	4590	GII	< 3	6.61 ± 0.62	< incomplete	incomplete	
Kepler-27 b	Tran.	0.105	0	5400	GII	< 3	3.94 ± 0.8	< incomplete	incomplete	bad phot.
Kepler-31 c	Tran.	0.255	0	6340	GII	< 3	34.64 ± 0.8	< incomplete	incomplete	NUV artifact
Kepler-47 b	Tran.	0.268		5636	GII	< 3	14.21 ± 1.27	< incomplete	incomplete	NUV artifact
Kepler-15 b	Tran.	0.057	0.66	5515	AIS	< 4	37.25 ± 3.87	< incomplete	incomplete	
Kepler-51 b	Tran.	0.248		5803	AIS	< 4	37.45 ± 5.57	< incomplete	incomplete	
Kepler-40 b	Tran.	0.081	2.18	6510	GII	–	–	–	–	edge
Kepler-6 b	Tran.	0.046	0.67	5647	AIS	< 4	74.85 ± 5.78	< incomplete	incomplete	
HD 187085 b	RV	2.028	0.8	6075	AIS	124.03 ± 9.15	sat.	-6.008 ± 0.032	–	
Qatar-1 b	Tran.	0.023	1.08	4861	AIS	< 4	19.6 ± 2.03	< -5.399	-4.622 ± 0.045	
GJ 785 b	RV	0.319	0.07	5144	AIS	54.19 ± 6.1	sat.	-7.073 ± 0.049	–	
HD 192699 b	RV	1.148	2.4	5220	AIS	17.36 ± 3.6	sat.	-7.255 ± 0.09	–	bad phot.
TrES-5 b	Tran.	0.025	1.77	5171	MIS	< 1	16.47 ± 2.14	< -5.598	-4.294 ± 0.056	
HAT-P-23 b	Tran.	0.023	2.09	5905	AIS	< 4	322.01 ± 10.78	< -5.599	-3.606 ± 0.015	NUV artifact
WASP-2 b	Tran.	0.031	0.9	5200	AIS	< 4	97.89 ± 3.81	< -5.748	-4.272 ± 0.017	
18 Del b	RV	2.575	10.21	4979	AIS	67.93 ± 5.98	sat.	-7.043 ± 0.038	–	
HD 200964 b	RV	1.597	1.84	5164	AIS	18.9 ± 4.37	sat.	-7.186 ± 0.1	–	bad phot.
BD +14 4559 b	RV	0.776	1.52	4814	NGS	1.07 ± 0.34	359.79 ± 1	-7.228 ± 0.137	-4.616 ± 0.001	NUV artifact
WASP-46 b	Tran.	0.024	2.08	5620	AIS	20.17 ± 3.66	258.54 ± 8.28	-4.546 ± 0.079	-3.352 ± 0.014	NUV artifact
HD 202206 b	RV	0.812	16.82	5788	AIS	24.95 ± 3.91	sat.	-6.377 ± 0.068	–	

Table 1—Continued

Star/Planet ^a ID	Disc. Method	a^b AU	M_p^b M_J	T_{eff}^b K	GALEX Survey	F_{FUV}^c μJy	F_{NUV}^c μJy	$\log(L_{FUV}/L_{bol})^d$	$\log(L_{NUV}/L_{bol})^d$	NOTE ^e
HD 204313 b	RV	3.071	3.5	5767	AIS	18.66 ± 3.66	sat.	-6.535 ± 0.085	—	
HD 204313 d	RV	3.945	1.61	5760	AIS	18.66 ± 3.66	sat.	-6.529 ± 0.085	—	
HD 205739 b	RV	0.895	1.49	6176	MIS	43 ± 1.3	sat.	-5.924 ± 0.013	—	
HAT-P-17 b	Tran.	0.088	0.53	5246	AIS	< 4	493.32 ± 8.74	< -6.243	-4.065 ± 0.008	
HD 206610 b	RV	1.633	2.23	4849	MIS	1.76 ± 0.44	956.69 ± 4.53	-7.542 ± 0.109	-4.721 ± 0.002	bad phot.
HD 209458 b	RV	0.047	0.69	6065	AIS	62.53 ± 5.29	sat.	-6.135 ± 0.037	—	
HD 210702 b	RV	1.203	1.96	5010	AIS	20.25 ± 4.41	sat.	-7.37 ± 0.095	—	
HD 212771 b	RV	1.064	2.25	4877	AIS	4.78 ± 1.99	sat.	-7.319 ± 0.181	—	
HD 212301 b	RV	0.034	0.4	5998	AIS	93.93 ± 5.18	sat.	-5.919 ± 0.024	—	4.3'' M3 comp. [6]
HD 213240 b	RV	1.885	4.53	5968	AIS	95.1 ± 6.71	sat.	-6.296 ± 0.031	—	
HD 215497 b	RV	0.047	0.02	5113	AIS	< 4	894.18 ± 10.26	< -6.871	-4.434 ± 0.005	NUV artifact
HAT-P-8 b	Tran.	0.045	1.29	6200	AIS	11.47 ± 2.88	sat.	-5.792 ± 0.109	—	
tau Gru b	RV	2.518	1.21	5999	AIS	211.28 ± 12.88	sat.	-6.254 ± 0.026	—	
HD 216437 b	RV	2.486	2.17	5849	AIS	120.01 ± 11.19	sat.	-6.505 ± 0.04	—	
HD 216770 b	RV	0.456	0.65	5423	GII	7.91 ± 0.66	sat.	-6.888 ± 0.036	—	
51 Peg b	RV	0.052	0.46	5787	AIS	190.68 ± 9.59	sat.	-6.543 ± 0.022	—	
HD 217107 b	RV	0.075	1.4	5704	AIS	44 ± 5.06	sat.	-6.898 ± 0.05	—	
HD 217786 b	RV	2.379	13.19	5966	GII	52.44 ± 1.35	sat.	-6.127 ± 0.011	—	
HD 218566 b	RV	0.687	0.21	4820	AIS	< 4	989.09 ± 19.03	< -7.08	-4.6 ± 0.008	
WASP-21 b	Tran.	0.052	0.3	5800	AIS	< 4	939.21 ± 15.5	< -5.786	-3.328 ± 0.007	
WASP-6 b	Tran.	0.043	0.52	5450	AIS	< 4	189.12 ± 7.66	< -5.649	-3.888 ± 0.018	
WASP-10 b	Tran.	0.038	3.19	4675	AIS	< 4	30.22 ± 3.24	< -5.517	-4.552 ± 0.047	
WASP-59 b	Tran.	0.07	0.86	4650	AIS	< 4	7.9 ± 3.05	< -5.547	-5.164 ± 0.167	NUV artifact
HD 219828 b	RV	0.052	0.06	5891	AIS	25.09 ± 3.93	sat.	-6.384 ± 0.068	—	
HD 220773 b	RV	4.943	1.45	5940	NGS	68.67 ± 2.18	sat.	-6.333 ± 0.014	—	
HD 221287 b	RV	1.25	3.12	6304	AIS	171.47 ± 9.23	sat.	-5.623 ± 0.023	—	
HD 222155 b	RV	5.139	2.03	5765	MIS	37.07 ± 4.66	sat.	-6.597 ± 0.055	—	
HD 222582 b	RV	1.337	7.63	5727	AIS	25.14 ± 2.85	sat.	-6.534 ± 0.049	—	
WASP-60 b	Tran.	0.053		5900	AIS	< 4	281.41 ± 8.18	< -5.538	-3.604 ± 0.013	
WASP-29 b	Tran.	0.046	0.24	4800	AIS	< 4	55.18 ± 2.77	< -6.033	-4.806 ± 0.022	
WASP-5 b	Tran.	0.027	1.62	5880	AIS	< 4	255.39 ± 6.95	< -5.499	-3.607 ± 0.012	
WASP-8 b	Tran.	0.08	2.14	5600	AIS	5.06 ± 1.66	1631.91 ± 12.75	-6.404 ± 0.142	-3.808 ± 0.003	NUV arti.; 4.8'' faint comp. [7]
HD 224693 b	RV	0.192	0.71	6037	AIS	27.31 ± 3.73	sat.	-6.261 ± 0.059	—	

^aTable ordered by R.A.

^bData are listed only for the inner most planet of the multi-planet systems. Masses are minimum masses for non-transiting planets. Planet and stellar parameters come from the Exoplanet Data Explorer (Wright et al. 2011).

^cFUV and NUV fluxes listed as “sat.” are saturated using the published counts-per-second limits per detector in Morrissey et al. (2007). These are 34 cps and 108 cps for the FUV and NUV detectors, respectively.

^dBolometric corrections, BC_K were calculated using Equations 17 and 18 of Masana et al. (2006). For those stars lacking literature values needed calculate BC_K , the fractional luminosities are left “incomplete”.

^eNotes on *GALEX* photometry. “Bad phot.” refers to a >20% difference in flux calculated using the “aper_auto” and “aper_7” apertures in the *GALEX* pipeline. “NUV artifact” refers to flags > 2 returned the the *GALEX* pipeline and should be used with caution. Binary blend are reported for those stars with relatively bright companions within 30”. Note that stars with any of these flags were not used in the analyses presented in this paper. The references for the close binaries are: [1] Raghavan et al. (2006), [2] Eggleton & Tokovinin (2008), [3] Patience et al. (2002), [4] Desidera et al. (2011), [5] Tamuz et al. (2008), [6] Mugrauer & Neuhäuser (2009), [7] Queloz et al. (2010).